Mediated Interactions beyond the Nearest Neighbor in an Array of Superconducting Qubits

Mediated Interactions beyond the Nearest Neighbor in an Array of Superconducting Qubits

Yariv Yanay,[1,*] Jochen Braumüller,[2] Terry P. Orlando,[2,3] Simon Gustavsson,[2] Charles Tahan,[1] and William D. Oliver[2,3,4,5]

[1] *Laboratory for Physical Sciences, 8050 Greenmead Dr., College Park, Maryland 20740, USA*
[2] *Research Laboratory of Electronics, Massachusetts Institute of Technology, Cambridge, Massachusetts 02139, USA*
[3] *Department of Electrical Engineering and Computer Science, Massachusetts Institute of Technology, Cambridge, Massachusetts 02139, USA*
[4] *Department of Physics, Massachusetts Institute of Technology, Cambridge, Massachusetts 02139, USA*
[5] *MIT Lincoln Laboratory, Lexington, Massachusetts 02421, USA*

(Received 8 November 2021; revised 3 March 2022; accepted 3 March 2022; published 25 March 2022)

We consider mediated interactions in an array of floating transmons, where each qubit capacitor consists of two superconducting pads galvanically isolated from ground. Each such pair contributes two quantum degrees of freedom, one of which is used as a qubit, while the other remains fixed. However, these extraneous modes can generate coupling between the qubit modes that extends beyond the nearest neighbor. We present a general formalism describing the formation of this coupling and calculate it for a one-dimensional chain of transmons. We show that the strength of coupling and its range (that is, the exponential falloff) can be tuned independently via circuit design to realize a continuum from nearest-neighbor-only interactions to interactions that extend across the length of the chain. We discuss how this coupling breaks integrability, allowing the system to locally equilibrate, and so enables exploration of quantum thermalization. We present designs with capacitance and microwave simulations showing that various interaction configurations can be achieved in realistic circuits. Such a coupling could be used in analog simulation of different quantum regimes or to increase connectivity in digital quantum systems. Thus the mechanism must also be taken into account in other types of qubits with extraneous modes.

DOI: 10.1103/PhysRevApplied.17.034060

I. INTRODUCTION

Superconducting quantum circuits are one of the leading experimental platforms in the quest for achieving larger-scale quantum processors [1]. Most recently, larger and increasingly complex circuits comprising lattices of qubits are being used in order to perform proof-of-principle demonstrations of quantum algorithms [2], quantum error correction [3], and simulations [4–9]. Most of these experiments take the form of a planar configuration of qubits, where coupling appears only between nearest-neighbor (NN) pairs. Longer-range coupling such as next-nearest neighbor (NNN) and beyond are commonly small, and are generally treated as parasitic interactions [10].

We consider here arrays of "floating" qubits, whose shunt capacitor is implemented by two floating electrodes. This is in contrast with "single-ended" qubits, which have one grounded electrode (e.g., Ref. [11]). The floating architecture has several advantages from an experimental point of view, including the decoupling of flux biasing lines, and is natural for experiments where the qubits have a nonlinear topology [12]. A fundamental difference between the two architectures is that a floating qubit has 2 quantum degrees of freedom, defined by the phase between the electrodes and their phase relative to ground. While direct capacitive coupling is substantial only between nearest-neighbor qubits, the set of extra quantum degrees of freedom present in floating qubit architectures can mediate longer-range coupling, as shown in Fig. 1(b). Note that these interactions are not mediated by the intervening *qubit* modes, and are not affected by their frequency detuning.

Such mediated interactions can be significant. Where they are not deliberate, they must be understood so that spurious coupling between the qubits is minimized. However, longer-range interactions can also be of interest for various applications in quantum computation, including simulating bosonic gases with rich phase diagrams [13], realizing the quantum approximate optimization algorithm (QAOA) [14], or efficiently generating the Porter-Thomas distribution, a hard quantum task [15]. With proper control,

*yariv@lps.umd.edu

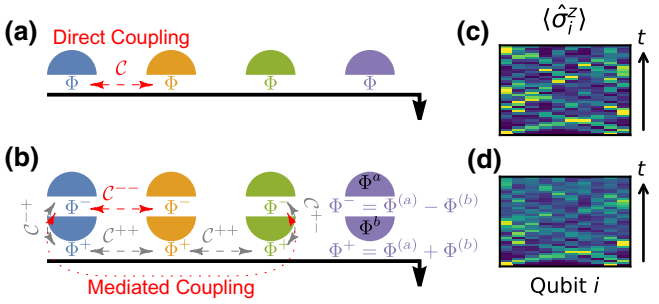

FIG. 1. We compare two designs for an array of superconducting qubits. (a) Each "single-ended" qubit is a single superconducting pad, whose phase difference to ground encodes the qubit. Different qubits are coupled by direct capacitance. (b) By contrast, "floating" qubits are made up of a pair of pads each (here shown in the same color), and so have 2 quantum degrees of freedom. The qubit is encoded in the phase difference between the pads, Φ^-, and these modes are again coupled to each other by direct capacitance. The average phase to ground, Φ^+, does not appear in any inductive element, and can be integrated away. However, because the "+" mode are coupled to the "−" modes and to each other, they mediate an effective interaction, which can extend beyond the nearest neighbor (NN). This coupling can fundamentally change the nature of the system; for example, a qubit chain with NN hopping is an integrable system: it retains a memory of its initial state. This is seen in (c), where a chain of ten qubits is initiated with two excitations, and their trajectories can be seen even at long times. By comparison, when the floating qubit array is initiated in the same state in (d), it quickly reaches local equilibrium. See Sec. IV for more detail.

they can also allow more efficient computation of digital circuits. Such interactions are also of interest in the study of localization, where they can, e.g., lead to a phase with a mobility edge [16]. Such models present a powerful tool for studying many-body localization and the eigenstate thermalization hypothesis [17,18], as well as entanglement dynamics [19]. Recent experiments in atomic physics using optical lattices have shown the power of this approach [20,21], but they have been limited in the parameter space that they can explore.

Here, we describe a design strategy for superconducting qubit lattices that enables control of this qubit-qubit coupling beyond the nearest neighbor. While such a long-range interaction is suppressed in single-ended qubit arrays, in a lattice of floating qubits we show the coupling strength can be controlled by adjusting the capacitance ratios in the circuit. Where the coupling between qubits i,j takes the form

$$J_{|i-j|} \approx J_1 \xi^{|i-j|-1}, \quad J_1 = \chi\omega, \tag{1}$$

the ratio of the NN coupling to the qubit frequency, χ, and the drop off of coupling strength with distance, ξ, can be independently adjusted by the capacitance ratios. We note that this nonlocal interaction does not require the complexity overhead of direct physical connections—the circuit contains only nearest-neighbor physical couplings—it is an effective coupling that can be adjusted by circuit design.

The remainder of the paper is organized as follows. In Sec. II we perform a circuit analysis for a system of floating qubits and give a general formulation for the mediated interaction terms. In Sec. III we calculate these coupling strengths for a one-dimensional chain and show how they can be adjusted. In Sec. IV we review how this system, as described, can be used to explore integrability and eigenstate thermalization. Finally, in Sec. V we demonstrate the experimental feasibility of such chains by performing capacitance simulation on their circuit designs.

II. CIRCUIT MODEL

We begin by performing circuit analysis for an array of qubits with two floating capacitor electrodes. We keep our discussion general to any qubit modality that uses a capacitive shunt and where the interactions between adjacent qubits of a lattice are implemented through capacitive coupling. For instance, this applies to the widely utilized transmon qubit [22] and the capacitively shunted flux qubit [23]. For simplicity, we first analyze a one-dimensional chain in our circuit analysis and then generalize our results to higher dimensions.

A. Circuit Hamiltonian

We consider the circuit shown in Fig. 2(a), a homogeneous one-dimensional chain of N transmons with two floating capacitor plates each. Following Ref. [24], we define node fluxes $\Phi_i^{(\sigma)}$ and node phases $\phi_i^{(\sigma)} = 2\pi\Phi_i^{(\sigma)}/\Phi_0$, for the qubit electrodes on the two sides of the Josephson junction, $\sigma = a, b$, of qubit i. Φ_0 is the magnetic flux quantum. The system Lagrangian takes the form

$$\mathcal{L} = \mathcal{T} - \mathcal{V}, \quad \mathcal{V} = -\sum_{i=1}^{N} E_J{}^{(i)} \cos(\phi_i^{(a)} - \phi_i^{(b)}), \tag{2}$$

where $E_J{}^{(i)}$ is the Josephson energy for qubit i. The kinetic energy is given by

$$\mathcal{T} = \sum_{i=1}^{N}\left[\frac{1}{2}C_q\left(\dot{\Phi}_i^{(a)} - \dot{\Phi}_i^{(b)}\right)^2 + \sum_{\sigma=a,\,b}\frac{1}{2}C_G\left(\dot{\Phi}_i^{(\sigma)}\right)^2\right] + \sum_{i=1}^{N-1}\frac{1}{2}C_c\left(\dot{\Phi}_i^{(b)} - \dot{\Phi}_{i+1}^{(a)}\right)^2. \tag{3}$$

As we see, the coupling properties of the circuit are controlled by the qubit capacitance C_q, the ground capacitance C_G, and the coupling capacitance between adjacent qubits, C_c.

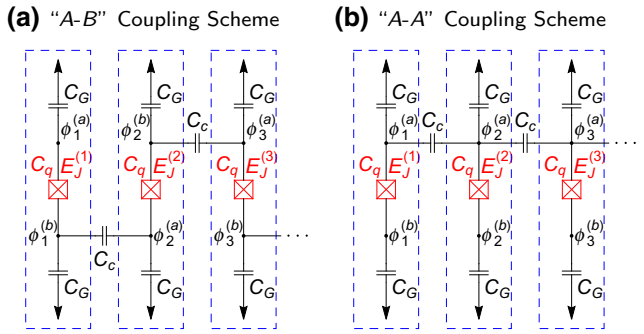

FIG. 2. Schematic circuit diagram for the one-dimensional chain of floating transmonlike qubits. Each qubit, outlined with a dashed blue line, has two independent circuit flux nodes, characterized by phases $\phi_i^{(a)}$, $\phi_i^{(b)}$, respectively. Nodes of the same qubit are coupled with a capacitance C_q, adjacent nodes of different qubits have a coupling capacitance C_c, and each node has a capacitance C_G to ground. The qubits have Josephson junctions with Josephson energies $E_J{}^{(i)}$. We show both (a) the "*A-B*"-coupling scheme, where the coupling elements are placed on alternating plates, and (b) the "*A-A*"-coupling scheme, where the coupling to the preceding and following qubit is done via the same capacitor plate. Each pattern can repeat indefinitely.

To recover the qubit degrees of freedom, we perform a variable transformation to "±" variables,

$$\Phi_i^{\pm} = \Phi_i^{(a)} \pm \Phi_i^{(b)}. \tag{4}$$

Note that the Josephson energy $\mathcal{V}$ is diagonal in terms of the phases $\phi_i^- \propto \Phi_i^-$, and so they define the qubit modes.

The kinetic energy in the new basis becomes

$$\mathcal{T} = \sum_{i=1}^{N} \left[\frac{1}{2}\frac{C_G}{2} \left(\dot{\Phi}_i^+\right)^2 + \frac{1}{2}\left(C_q + \frac{C_G}{2}\right)\left(\dot{\Phi}_i^-\right)^2 \right] + \sum_{i=1}^{N-1} \frac{1}{2}\frac{C_c}{4}\left(\dot{\Phi}_i^+ - \dot{\Phi}_i^- - \dot{\Phi}_{i+1}^+ - \dot{\Phi}_{i+1}^-\right)^2. \tag{5}$$

To elucidate the contributions of these modes to the chain's coupling behavior, it is useful to rewrite the kinetic energy in matrix form, separating "+" and "−" variables and their respective capacitance matrices,

$$\mathcal{T} = \frac{1}{2}\begin{pmatrix}\dot{\Phi}^+\\ \dot{\Phi}^-\end{pmatrix}^T \begin{pmatrix}\mathcal{C}^{++} & \mathcal{C}^{+-}\\ \mathcal{C}^{-+} & \mathcal{C}^{--}\end{pmatrix}\begin{pmatrix}\dot{\Phi}^+\\ \dot{\Phi}^-\end{pmatrix}. \tag{6}$$

Here, $\Phi^{\pm} = (\Phi_1^{\pm}, \Phi_2^{\pm}, \dots)^T$ and the submatrices $\mathcal{C}^{\pm\pm}$ are defined by equating Eqs. (5) and (6). A Legendre transformation yields the circuit Hamiltonian

$$\mathcal{H} = \frac{1}{2}\begin{pmatrix}\mathbf{q}^+\\ \mathbf{q}^-\end{pmatrix}^T \begin{pmatrix}\mathcal{C}^{++} & \mathcal{C}^{+-}\\ \mathcal{C}^{-+} & \mathcal{C}^{--}\end{pmatrix}^{-1}\begin{pmatrix}\mathbf{q}^+\\ \mathbf{q}^-\end{pmatrix} + \mathcal{V}, \tag{7}$$

where $\mathbf{q}^{\pm} = (q_1^{\pm}, q_2^{\pm}, \dots)$.

Note that due to the absence of inductive terms including ϕ_i^+ in the Hamiltonian of Eq. (7), the charges q_i^+ remain static. The "+" modes can thus be traced out by demoting q_i^+ to constants, and we find the effective Hamiltonian containing only "−" modes to be

$$\hat{H} = \frac{1}{2}\hat{\mathbf{q}}^-\,\mathcal{C}_{\text{eff}}{}^{-1}\,\hat{\mathbf{q}}^- - E_J\sum_{i=1}^{N}\cos\hat{\phi}_i^-, \tag{8}$$

where we now promote the variables to operators. The effective capacitance matrix $\mathcal{C}_{\text{eff}}$ of the reduced circuit can be found by taking the bottom-right quadrant of the inverse matrix in Eq. (7), and it is given by

$$\mathcal{C}_{\text{eff}} = \mathcal{C}^{--} - \mathcal{C}^{-+}\cdot(\mathcal{C}^{++})^{-1}\cdot\mathcal{C}^{+-}. \tag{9}$$

Comparing this effective capacitance matrix with the capacitance matrix of a chain of single-ended qubits (see Appendix A), we observe that in addition to the direct capacitance between the qubit "−" modes described by $\mathcal{C}^{--}$, it contains an additional contribution mediated by the "+" modes.

As detailed below, this hidden degree of freedom mediates long-range interactions in the chain independently of qubit frequencies, enabling us to tailor the long-range interactions.

Note that while we use the transmon design of Fig. 2(a) for concreteness, Eqs. (6)–(9) are in fact quite generic, and the effective capacitance formalism can be used in higher-dimensional architectures, or even for different qubit modalities, as long as the ϕ_i^+ do not appear in any of the inductive terms of $\mathcal{V}$. This means it can be used for other qubit modalities with extraneous degrees of freedom, such as fluxonium [25] or the $0-\pi$ qubit [26].

Alternative approaches to extract qubit-qubit couplings in weakly anharmonic circuits are based on extracting their impedance matrix [27,28].

B. Qubit-qubit coupling strength

To extract the coupling strength between various pairs of qubits in the chain, it is useful to rewrite Eq. (8) as

$$\hat{H} = \sum_i \hat{H}_i^Q + \sum_{i=1}^{N-1}\sum_{j=i+1}^{N}\hat{H}_{ij}^c. \tag{10}$$

The first term represents the single-qubit Hamiltonians $\hat{H}_i^Q$, which contains the diagonal terms of the capacitance matrix in Eq. (9) and can be expressed in terms of the charging energy $4E_C{}^{(i)} = 2e^2(\mathcal{C}_{\text{eff}}{}^{-1})_{ii}$,

$$\hat{H}_i^Q = 4E_C{}^{(i)}\hat{n}_i^2 - E_J{}^{(i)}\cos\hat{\phi}_i^-. \tag{11}$$

The second term in Eq. (10), which we identify as a coupling Hamiltonian, contains the off-diagonal matrix

elements $g_{ij} = (2e)^2(\mathcal{C}_{\text{eff}}{}^{-1})_{ij}$,

$$\hat{H}^c_{ij} = g_{ij}\hat{n}_i\hat{n}_j. \tag{12}$$

Here, $\hat{n}_i = \hat{q}_i^-/2e$ and $\hat{\phi}_i^-$ form the conjugate pair of Cooper-pair number operator and phase operator, respectively, associated with qubit i.

Using the set of basis vectors $\{|\epsilon\rangle_i\}$ in the excitation basis of the qubits, $\hat{H}_i^Q |\epsilon\rangle_i = \epsilon |\epsilon\rangle_i$, the number operators can be expressed as

$$\hat{n}_i = \sum_{\epsilon,\epsilon'} \langle\epsilon|\hat{n}_i|\epsilon'\rangle_i \; |\epsilon\rangle\langle\epsilon'|_i, \tag{13}$$

such that the coupling strengths between the fundamental transitions of qubits i,j become

$$J_{ij} = g_{ij}\langle g|\hat{n}_i|e\rangle_i\langle e|\hat{n}_j|g\rangle_j \tag{14}$$

and its Hamiltonian can be written, for the first two levels

$$\hat{H}^c_{ij} \approx \hat{H}^{xx}_{ij} = J_{ij}\sigma_i^+\sigma_j^- + J_{ji}\sigma_j^+\sigma_i^-. \tag{15}$$

States $|g\rangle$, $|e\rangle$ denote the ground and first excited state of the qubit, respectively, and we discard counter-rotating terms and corrections to the qubit frequency.

In the transmon regime, $E_J \gg E_C$ [22], the ratio of the coupling energy to the qubit frequency for identical qubits i,j is proportional to the ratio of the coupling matrix elements,

$$\frac{J_{ij}}{\omega_i} = \frac{g_{ij}}{16{E_C}^{(i)}} + O\left(\sqrt{{E_C}^{(i)}/{E_J}^{(i)}}\right), \tag{16}$$

where we approximate the qubit frequency $\omega_i \approx \sqrt{8{E_J}^{(i)}{E_C}^{(i)}}$ and $|\langle e|n_i|g\rangle| \approx ({E_J}^{(i)}/32{E_C}^{(i)})^{1/4}$.

We note that in a superconducting circuit, the capacitance is generally fixed, and therefore so are $\mathcal{C}_{\text{eff}}$ and the coupling elements g_{ij}. This makes the physical coupling between qubits hard to tune. However, the qubit's frequency, which depends on ${E_J}^{(i)}$, can often be controlled. The effective coupling between qubits can thus be controlled by putting them into and out of resonance, allowing this long-range interaction to be turned on and off at will. Note that because the interaction is mediated by the "+" modes, this interaction strength *does not* depend on the frequency of intermediate qubits, which can thus be detuned away while longer-range coupling persists.

C. Characterizing the coupling

To analyze the coupling generated by $\hat{H}^{xx}$, we introduce two dimensionless parameters inspired by Eq. (1).

First, we define the relative coupling strength as the ratio of the NN qubit coupling to the qubit frequency,

$$\begin{aligned}\chi_i &\equiv \sqrt{\left|(\mathcal{C}_{\text{eff}}{}^{-1})_{i,i+1}(\mathcal{C}_{\text{eff}}{}^{-1})_{i,i-1}\right|}/2(\mathcal{C}_{\text{eff}}{}^{-1})_{ii} \\ &= \sqrt{\left|g_{i,i+1}g_{i,i-1}\right|}/16{E_C}^{(i)} \approx \sqrt{\left|J_{i,i+1}J_{i,i-1}\right|}/\omega_i,\end{aligned} \tag{17}$$

As we generally expect coupling strength to fall off with distance, the NN term serves as a proxy for overall coupling strength.

Second, we define the damping factor as the fall off in strength between the NN and NNN coupling,

$$\xi_i \equiv \sqrt{\left|\frac{(\mathcal{C}_{\text{eff}}{}^{-1})_{i,i+2}(\mathcal{C}_{\text{eff}}{}^{-1})_{i,i-2}}{(\mathcal{C}_{\text{eff}}{}^{-1})_{i,i+1}(\mathcal{C}_{\text{eff}}{}^{-1})_{i,i-1}}\right|} = \sqrt{\left|\frac{J_{i,i+2}J_{i,i-2}}{J_{i,i+1}J_{i,i-1}}\right|}. \tag{18}$$

In the case of an exponential drop off, as in the one-dimensional chain we analyze below, ξ is the decay constant.

For a uniform, infinite chain, ${E_C}^{(i)} = E_C, {E_J}^{(i)} = E_J$, translational invariance makes these parameters invariant as, $\chi_i \to \chi$ and $\xi_i \to \xi$. These then reduce to the form of Eq. (1). As we show in Sec. III D, this applies in the case of a long chain as well.

III. TUNING COUPLING STRENGTH IN A QUBIT CHAIN

Next, we evaluate the one-dimensional chain described in Sec. II and analytically calculate the coupling strength ratio χ and damping rate ξ as a function of the circuit capacitances C_G, C_q, and C_c.

We begin by writing out the capacitance matrices defined by Eq. (6). To simplify the calculation, we take $N \to \infty$, and find

$$\mathcal{C}^{++}_{ij} = \left[\frac{C_G}{2} + \frac{C_c}{2}\right]\delta_{i,j} - \frac{C_c}{4}\delta_{|i-j|,1}, \tag{19a}$$

$$\mathcal{C}^{--}_{ij} = \left[C_q + \frac{C_G}{2} + \frac{C_c}{2}\right]\delta_{i,j} + \frac{C_c}{4}\delta_{|i-j|,1}, \tag{19b}$$

$$\mathcal{C}^{+-}_{ij} = \frac{C_c}{4}(\delta_{i,j+1} - \delta_{j,i+1}), \tag{19c}$$

where $\delta_{i,j} = 1$ if $i = j$ and 0 otherwise.

A. Effective capacitance

To calculate the effective capacitance induced by the mediating modes, we must invert $\mathcal{C}^{++}$. We use a Fourier

transform,

$$\tilde{\mathcal{C}}^{++}(k,p) = \sum_{m,n} U_m(k)\mathcal{C}^{++}_{mn}U^*_n(p), \quad U_m(k) = e^{-ikm} \tag{20}$$

for $-\pi \leq k \leq \pi$, to express $\mathcal{C}^{++}$ in momentum basis,

$$\tilde{\mathcal{C}}^{++}(k,p) = \delta(k-p)\left(\frac{C_G}{2} + C_c \sin^2\frac{k}{2}\right), \tag{21}$$

where it is diagonal and can be immediately inverted. Using the inverse Fourier transform we can then return to the lattice basis, finding $(\mathcal{C}^{++})^{-1}_{ij}$, and substituting into Eq. (9) we find

$$(\mathcal{C}_{\text{eff}})_{ij} = C_q\delta_{i,j} + C_{c,\text{eff}}\xi_C^{|j-i|}, \tag{22}$$

where

$$C_{c,\text{eff}} = \sqrt{\frac{C_G}{2}\left(C_c + \frac{C_G}{2}\right)}, \tag{23a}$$

$$1/\xi_C = \left(\sqrt{\frac{C_G}{2C_c}} + \sqrt{1 + \frac{C_G}{2C_c}}\right)^2. \tag{23b}$$

We observe that interaction mediated by the "+" modes generates an effective capacitance, which starts at magnitude $C_{c,\text{eff}}$ for NN qubit pairs and drops off with factor ξ_C. A stronger coupling to ground, C_G, increases the energy of the mediating modes and thus reduces their range, while in the limit $C_G/C_c \to 0$ they generate infinite range capacitance between the "−" modes.

It is notable that the coupling strength and drop-off parameters depend on the product and the ratio of C_G and C_c, respectively, allowing the two to be tuned independently.

In the typical working regime, where the dominant term is the qubit capacitance, $C_q \gg C_G, C_c$, the coupling terms are simply given by the effective capacitance, suppressed by C_q,

$$\left(\mathcal{C}_{\text{eff}}^{-1}\right)_{ij} \approx \frac{1}{C_q}\delta_{i,j} - \frac{C_{c,\text{eff}}}{{C_q}^2}\xi_C^{|i-j|}, \tag{24}$$

and so the coupling parameters are

$$\chi_i \approx \frac{C_c}{8C_q}\frac{1-\xi_C^2}{\xi_C}, \quad \xi_i = \xi_C. \tag{25}$$

The calculation above can be repeated for the alternative coupling structure shown in Fig. 2(b). We find a similar expression in this case,

$$(\mathcal{C}_{\text{eff}})^{A-A}_{ij} = \left(C_q + C_G\right)\delta_{i,j} - \frac{{C_G}^2}{4C_{c,\text{eff}}}\xi_C^{|j-l|}, \tag{26}$$

or

$$\chi_i^{A-A} \approx \frac{C_c}{8C_q}\frac{1-\xi_C^2}{\xi_C}\left(\frac{1-\xi_C}{1+\xi_C}\right)^2, \quad \xi_i^{A-A} = \xi_C. \tag{27}$$

Here, the drop-off factor remains the same as in Eq. (22), but overall coupling strength is smaller. This means that at a fixed ground capacitance, the physical coupling capacitance C_c required to achieve some NN coupling strength J will lead to *larger* higher-order terms. In addition, the sign of the off-diagonal terms is negative here, which means the coupling terms in the qubit basis will be *positive*.

B. Strong coupling regime

While it is uncommon experimentally, it is possible to operate the chain in the strong coupling regime, $C_q \sim C_G, C_c$. Here, the full matrix must be used to estimate the coupling strength. One finds that the inverse capacitance matrix, and thereby the coupling terms, are

$$(\mathcal{C}_{\text{eff}}^{-1})_{ij} = \frac{1}{C_{q,\text{eff}}}\left[\delta_{i,j}\left(1 + \frac{2\chi}{\xi}\right) - \frac{2\chi}{\xi}\xi^{|i-j|}\right]. \tag{28}$$

The details of the calculation and the relations between the parameters χ, ξ and the capacitances C_q, C_c, C_G are given in Appendix B.

As defined in Eq. (28), χ, ξ are the relative coupling strength and interaction damping ratio of Eqs. (17) and (18), respectively. As before, the floating transmon circuit enables independent tuning of both parameters by setting the circuit capacitances C_q, C_c, C_G. For arbitrary values of $C_{q,\text{eff}} = e^2/2E_C$, we can tune χ and ξ in the ranges

$$0 \leq \xi \leq 1, \quad 0 \leq \chi \leq \frac{1-\xi}{4} \tag{29}$$

by choosing

$$C_q = \frac{\xi}{\xi + 2\chi}C_{q,\text{eff}}, \tag{30a}$$

$$C_c = \frac{8\chi}{1-(\xi+4\chi)^2}C_{q,\text{eff}}, \tag{30b}$$

$$C_G = \frac{4(1-\xi)\chi}{(\xi+2\chi)(1+\xi+4\chi)}C_{q,\text{eff}}. \tag{30c}$$

A similar calculation can be followed for the alternative circuit design of Fig. 2(b), yielding

$$(\mathcal{C}_{\text{eff}}^{-1})^{A-A}_{ij} = \frac{1}{C_{q,\text{eff}}}\left[\delta_{i,j}\left(1 - \frac{2\chi}{\xi}\right) + \frac{2\chi}{\xi}\xi^{|i-j|}\right], \tag{31}$$

$$0 \le \xi \le 1, \quad 0 \le \chi \le \frac{\xi(1-\xi)}{4}. \tag{32}$$

This design is more limited in the strong coupling regime, with the overall coupling strength bounded for small ξ. Similarly, for the fixed transmon described in Appendix A, we find

$$(\mathcal{C}_{\text{eff}}{}^{-1})_{ij}^{\text{fixed}} = \frac{1}{C_{q,\text{eff}}}\xi^{|i-j|}, \tag{33}$$

essentially fixing $\chi = \xi/2$.

C. Boundary effects

Finally, we consider the effects of a finite chain of length N on the coupling. The capacitance matrix acquires boundary terms, becoming

$$\mathcal{C}_{ij}^{++} = \left[\frac{C_G}{2} + \frac{C_c}{4}(2 - \delta_{i,1} - \delta_{i,N})\right]\delta_{i,j} - \frac{C_c}{4}\delta_{|i-j|,1}. \tag{34}$$

The calculation above can be repeated, as shown in Appendix C, to find that for large but finite N the effective capacitance matrix becomes

$$(\mathcal{C}_{\text{eff}})_{ij} \approx C_q\delta_{i,j} + C_{c,\text{eff}}\left(\xi_C^{|j-l|} - \xi_C^{N-|i+j-N-1|}\right), \tag{35}$$

with $C_{c,\text{eff}}, \xi_C$ as defined in Eq. (23). We see that the boundary effects have the same geometric drop-off factor, ξ_C from the edges of the chain as the one that controls the length of the interaction.

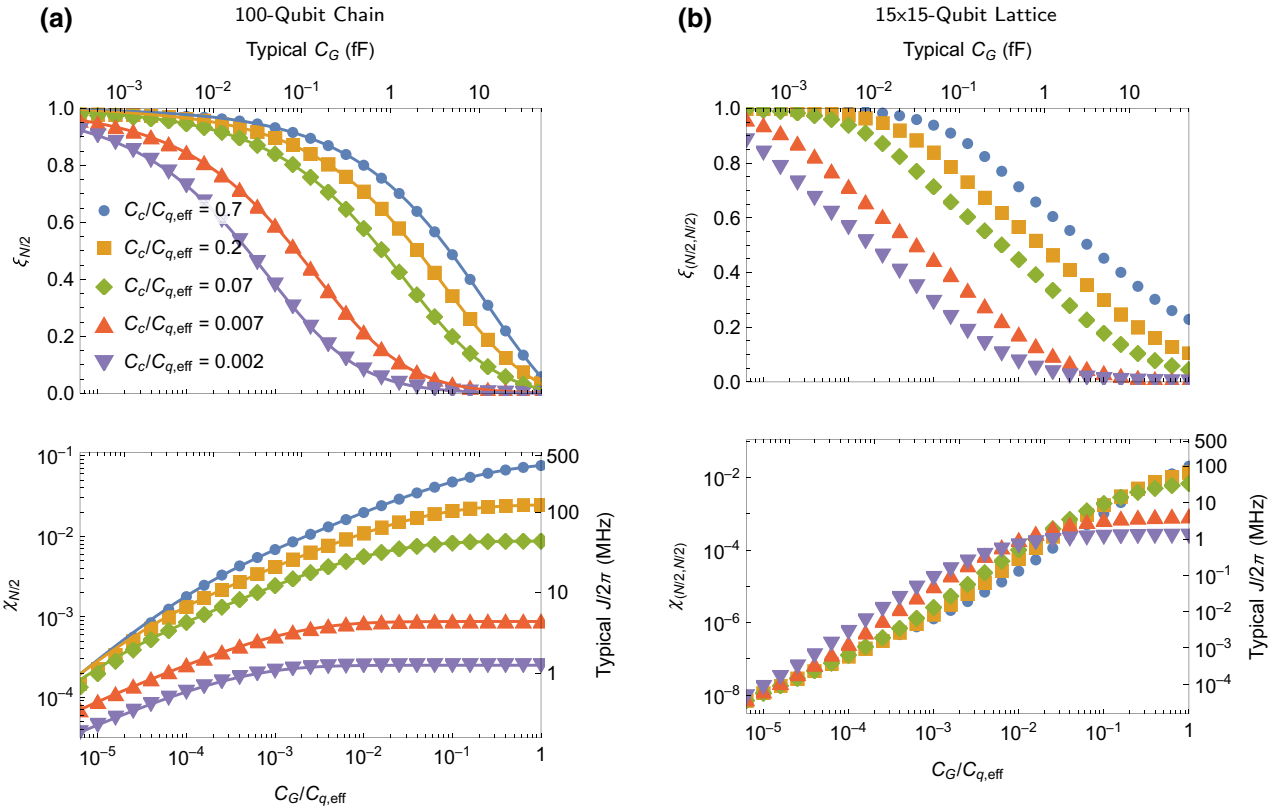

FIG. 3. The coupling parameters χ and ξ, as a function of the capacitance ratios. We fix the qubit frequency by keeping $C_{q,\text{eff}} \propto E_C{}^{-1}$ constant, and vary C_G, C_c. (a) Shown for an $N = 100$ chain each composed of floating qubits with "*A*-*B*" coupling, as shown in Fig. 2(a). The solid lines are the analytical results derived from Eq. (35). The points show numerical results for for χ_{50}, ξ_{50}, at the center of a chain of $N = 100$ qubits. The two plots share a horizontal axis, shown at the bottom as the ratio $C_G/C_{q,\text{eff}}$ and at the top as values of C_G for a typical system with $C_{q,\text{eff}} = 50$ fF ($E_C/2\pi \approx 400$ MHz). Top: the interaction damping ξ can be tuned between an approximate nearest-neighbor coupling regime and almost all-to-all coupling by varying C_G. Bottom: a large range of coupling strengths χ is accessible for each value of ξ by adjusting C_c. Recall from Eq. (17) that the NN coupling strength is given by $J/\omega = \chi$, where ω is the qubit frequency; the right-hand axis shows NN coupling strength for a qubit operating at $\omega/2\pi = 5$ GHz. We observe that the numerical results agree with the analytic formula. (b) A similar plot is shown for a 15×15 square lattice composed of floating qubits with "*A*-*A*" coupling, where we find the exponential drop-off picture to be simple. In other configurations, we observe a more complex form, with $J_{i,j}$ varying differently in different direction, see Appendix D for details.

D. Numerical results

Figure 3 summarizes numerical results for the interaction damping ξ and the coupling strength χ dependent on the circuit capacitances C_G, C_q, and C_c as given in Fig. 2(a) ("*A*-*B*" coupling). We plot χ_i, ξ_i for $i = N/2$, at the center of the chain, where boundary effects are small. Numerical simulations are presented for a qubit chain of length $N = 100$. While varying the circuit capacitances, we fix the effective qubit capacitance $C_{q,\text{eff}} \propto {E_C}^{-1}$, such that the qubit transition frequencies and their anharmonicities are constant. For $C_G/C_q \lesssim 10^{-3}$, this results in a physical $C_q \approx C_{q,\text{eff}}$, while for larger $C_G/C_q \lesssim 1$ one finds $0.5 \lesssim C_q/C_{q,\text{eff}} < 1$.

As noted above, the drop-off rate can be adjusted between $\xi = 0$, the asymptotic nearest-neighbor coupling regime, and $\xi \approx 1$, where the connectivity extends far beyond that, by varying the capacitance ratio C_G/C_q. Changing the relative coupling capacitance C_c/C_q in the circuit yields similar results, approximately spanning the entire parameter range $0 < \xi < 1$. Therefore, C_c remains as a tuning knob for the nearest-neighbor coupling strength $J \equiv J_{i,i+1}$, as demonstrated in Fig. 3. J is exponentially suppressed for small C_G/C_q, but is nonzero in the entire parameter regime. An intuitive picture for the vanishing interaction strength χ at $C_G/C_q \to 0$ is that the effective dipole moment of the qubit vanishes.

Thus, we can set the long-range interaction damping rate ξ by varying the ratio C_G/C_q, and subsequently choose the nearest-neighbor coupling strength χ by adjusting C_c, while preserving the single-qubit properties, by keeping $E_C = \text{const}$.

Our numerical study also verifies the analytic properties described in Sec. III, including weak boundary effects and an exponential decay of the coupling described by $J_{i,j} \propto \xi^{|i-j|}$.

IV. EXPLORING THERMALIZATION AND INTEGRABILITY

The one-dimensional qubit chain with varying hopping length presented above can be immediately used to explore the subject of quantum thermalization.

An isolated quantum system prepared in a nonthermal state does not, on its own, reach a thermal equilibrium. However, if it is initially prepared in some pure state that is not an eigenstate of the system, such systems may appear to thermalize *locally*, with the rest of the system acting as a bath for any small subsystem, an idea known as the eigenstate thermalization hypothesis [29].

This hypothesis does not apply equally to all systems. One particularly interesting class of models, which do not thermalize, are so-called integrable models [30,31], which have an extensive number of local integrals of motion. These systems, and the crossover from integrability to thermalization, have been of interest to physicists for a long time, both theoretically and experimentally [32–36]

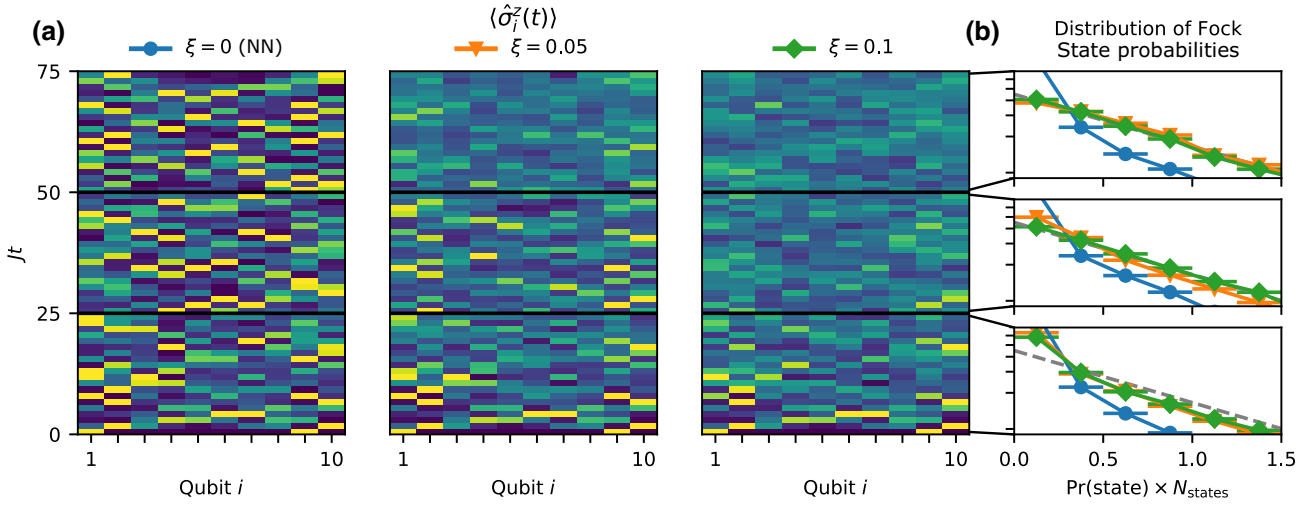

FIG. 4. Integrability versus thermalization in an $N = 10$ qubit chain. In a numerical simulation, the system is initially prepared in the state $|\Psi(0)\rangle = \hat{\sigma}_1^+\hat{\sigma}_{N-1}^+|0\rangle^{\otimes N}$ and allowed to evolve under a Hamiltonian with hopping at strength falling off with distance at $\xi = 0$ (NN hopping only), 0.05, 0.1. (a) We plot the average occupation $\langle\hat{o}_i^z\rangle$ of each qubit from the initial preparation to a long time $Jt = 25$. In the NN case one can clearly see particlelike trajectories, which do not thermalize over time, while for $\xi = 0.1$, the occupation numbers quickly become diffuse. In the intermediate case, $\xi = 0.05$, we observe the trajectories give way to diffuse occupation over time. (b) Logarithmic scale histograms show how often one finds a Fock state to have some probability Pr at early, intermediate, and late times, $Jt \in (0, 25), (25, 50), (50, 75)$, respectively. In a thermalized quantum system, these probabilities are sampled from the Porter-Thomas distribution, $N_{\text{counts}} \propto \exp(-\text{Pr} \times N_{\text{states}})$, shown by a dashed gray line. We observe the system with hopping beyond the nearest-neighbor approach this distribution, while the integrable NN chain remains unthermalized.

Notably, this class of system includes the one-dimensional qubit chain with NN hopping, which is equivalent to a free fermion model via a Jordan-Wigner transformation. The addition of coupling beyond the nearest neighbor, as in Eq. (1), breaks the integrability of the system, allowing it to locally thermalize. We show this effect in a small, $N = 10$ chain, numerically, in Fig. 4.

In the absence of hopping beyond the NN, the one-dimensional chain is equivalent to the integrable free-fermion chain. In this case, the system remembers information about its initial state even at very long times, and the distribution of Fock-state probabilities remains in its nonthermalized form. One can trace the trajectories of two particlelike excitations, in a form reminiscent of the quantum Newton's cradle [32]. When couplings beyond the NN are turned on, the system tends towards thermalization, as the excitation density map is smoothed out and the probabilities of individual states occur at rates sampled from a Porter-Thomas distribution [37,38].

One exciting possibility brought about by the tuneable parameters is the ability to go between these two regimes. In the intermediate regime shown in Fig. 4, at $\xi = 0.05$, one can see that a locally thermal form is reached, but only after a longer time period. The mechanism suggested in Sec. III could allow experimental realization of these models at a highly controllable manner, where both the coupling range ξ and the initial state $|\Psi(0)\rangle$ could be tuned beyond what is easily achievable in atomic systems.

We note that while these systems are easy to simulate at a low occupation number (e.g., two excitations in Fig. 4) they are exponentially hard to calculate at finite fractional (e.g., half) filling. Calculating the evolution of a 20-qubit chain from an initial state with ten excited qubits would be prohibitively hard on a classical computer, but easily within grasp of current experimental setups. Such computationally difficult tasks are aided by higher connectivity [15]. These same systems could also be used in exploration of information scrambling and quantum scarring [12,39].

V. ACCESSIBLE REGIMES IN CIRCUIT DESIGN

In this section, we consider the experimental feasibility of tailoring the nearest-neighbor coupling and long-range interaction parameters χ and ξ in a wide parameter range via microwave simulations of two sample circuits, chosen to exhibit two different parameter regimes.

We investigate two circuits, each comprising a one-dimensional chain of seven qubits, see Fig. 5, and we extract χ and ξ from the central five qubits, referred to as Q1 through Q5. The qubits at the edge of the lattice suppress boundary effects.

To analyze each circuit, we first perform a dc capacitance matrix simulation using ANSYS Maxwell. This enables us to numerically calculate the coupling strength χ and the interaction damping ξ for the specific circuit, using Eqs. (17) and (18). We subsequently confirm both

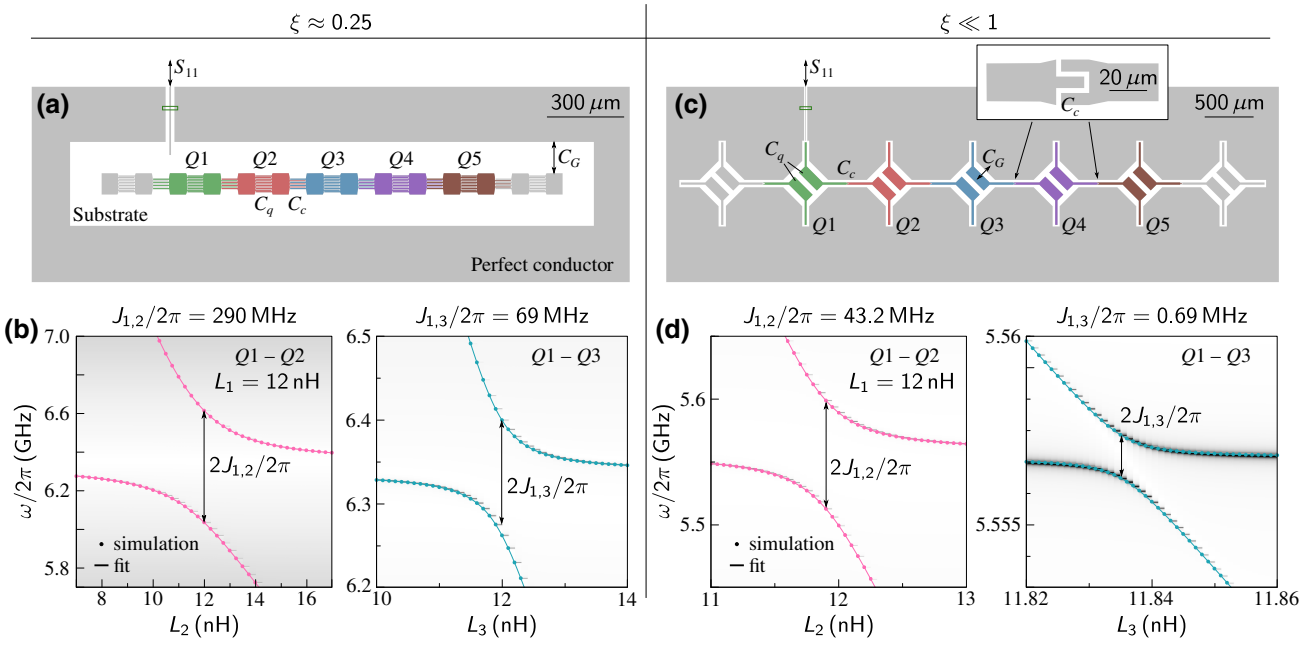

FIG. 5. Schematic circuit diagram for the one-dimensional chain of transmonlike qubits with two floating capacitor pads. We show two designs: (a),(b) a moderate falloff, $\xi \approx 0.25$, between NN and NNN coupling, (c),(d) a traditional design with negligible NNN coupling, $\xi \ll 1$. (a),(c) show the circuit realization, where electrodes belonging to the same qubit are equally colored for clarity. (b),(d) show the simulated spectrum, including the effective NN coupling (between Q1, Q2) and NNN coupling (between Q1, Q3).

TABLE I. Summary of the interaction parameters calculated numerically based on the simulated circuit capacitances and for the microwave simulation of the two sample layouts depicted in Fig. 5.

Design		$\omega_1/2\pi$ (GHz)	$J_{12}/2\pi$ (MHz)	$J_{13}/2\pi$ (MHz)	$J_{14}/2\pi$ (MHz)	$J_{15}/2\pi$ (MHz)	χ	ξ
$\xi \approx 0.25$	Simulation	6.336 $\pm 1.1 \times 10^{-5}$	289.5 ± 0.05	68.65 ± 0.02	17.57 ± 0.007	4.60 ± 0.03	0.0457 $\pm 8 \times 10^{-6}$	0.2374 $\pm 1.8 \times 10^{-4}$
	Calculation	6.013	279.3	69.45	17.26	4.23	0.0464	0.249
$\xi \ll 1$	Simulation	5.557 $\pm 7 \times 10^{-7}$	43.2 $\pm 6 \times 10^{-3}$	0.686 $\pm 8 \times 10^{-4}$	0.145 6×10^{-4}	0.041 1.5×10^{-4}	0.0078 ± 0.0011	0.016 $\pm 1.9 \times 10^{-5}$
	Calculation	5.434	46.31	0.18	7×10^{-4}	3×10^{-6}	0.0085	0.0039

parameters with microwave simulations using Sonnet. In the Sonnet simulations, we treat the qubits as harmonic oscillators and replace their Josephson junctions with linear ideal-element inductors with an inductance of 12 nH. This is valid since the investigated effect is not dependent on the inductance in the circuit, as pointed out in Sec. II.

We probe the spectrum of the qubit chain by simulating microwave reflection at a port connected to an antenna that weakly couples to Q1, see Figs. 5(a) and 5(c). We then extract the coupling strength J_{12} (J_{13}, J_{14}, J_{15}) between Q1 and Q2 (Q3, Q4, Q5) in a simulation with zero inductance for all qubits except the pair considered, effectively removing them as circuit modes but preserving their capacitive contribution. By sweeping the inductance of one of the qubits forming a pair, respectively, we observe an avoided level crossing in the simulated spectrum, enabling us to extract the coupling strength from the minimal separation, see Figs. 5(b) and 5(d).

We first investigate a circuit implementation with a slow interaction decay rate $\xi \approx 0.25$, as depicted in Fig. 5(a). The qubit capacitor pads are far away from the surrounding ground metallization, resulting in a small $C_G = 16.8$ fF. The qubit capacitance $C_q = 42.3$ fF and the capacitance between adjacent qubits $C_c = 27.4$ fF are larger, due to the large interdigital finger capacitors. The nearest-neighbor coupling strength $J_{1,2}$ and the next-nearest-neighbor coupling strength $J_{1,3}$ are extracted according to Fig. 5(b) and the resulting interaction parameters up to distance four are summarized in Table I. The transition and coupling frequencies we obtain from the capacitance and microwave simulations are within 5% of each other, with the difference explained by the fact that the dc capacitance simulation cannot account for all microwave effects in the circuit. Since the interaction parameters χ and ξ are ratios of the extracted frequencies, we find good agreement between the two simulations.

To demonstrate that the long-range interactions can be suppressed, we analyze the circuit in Fig. 5(c), featuring large ground capacitances $C_G = 112$ fF but smaller $C_q = 13.3$ fF, $C_c = 4.88$ fF. From the coupling strengths extracted in Fig. 5(d), we find that the coupling strength falls off much faster (see Table I), demonstrating that the long-range interaction can be strongly suppressed by circuit design. While the coupling strength χ is in good agreement in both simulations, the predicted ξ based on the simulated dc circuit capacitances is notably smaller. We attribute this discrepancy to long-range capacitive coupling channels, which are not taken into account in the calculation but manifest in the microwave simulation, and become significant for the small coupling J_{13}, J_{14}, J_{15}.

VI. CONCLUSIONS

We analyze arrays of floating superconducting qubits, showing that beyond direct capacitive coupling the qubit modes are subject to additional interactions, mediated through otherwise-static "+" modes.

We demonstrate that the drop off in coupling strength in a chain of floating qubits can be adjusted by circuit design, independently from the effective qubit capacitance and NN coupling strength. This is in contrast with single-ended qubit realizations, where the drop off is determined by these parameters. The coupling strength can be tailored via circuit design from asymptotically approaching zero to dropping off at a rate $1 - \xi \sim 1/N$, generating quasi-all-to-all coupling without adding direct connections.

The implementation of longer-ranged coupling has potential uses in many applications, including QAOA and quantum simulation. It may also be interesting to consider the interplay of these modes with direct capacitive coupling beyond the nearest neighbor [40]. In addition, the mediated interaction mechanism we show here may be significant in other applications where extraneous quantum modes exist but are not used as part of the qubit, including the fluxonium [25] and $0 - \pi$ [26] qubits. There they can be considered either as a resource to utilize, but also as a potential source of unwanted interactions between the qubits.

ACKNOWLEDGMENTS

The authors are grateful to A. Stehli for providing fitting code used in extracting the coupling strengths.

This research is funded in part by the Office of the Director of National Intelligence (ODNI), Intelligence Advanced Research Projects Activity (IARPA), and the Department of Defense (DoD) via MIT Lincoln Laboratory under Air Force Contract No. FA8721-05-C-0002. The views and conclusions contained herein are those of the authors and should not be interpreted as necessarily representing the official policies or endorsements, either expressed or implied, of the ODNI, IARPA, the DoD, or the U.S. Government.

J.B. and Y.Y. contributed equally to this work.

APPENDIX A: LONG-RANGE INTERACTIONS IN A LATTICE OF SINGLE-ENDED QUBITS

We calculate here the qubit coupling in a one-dimensional chain of single-ended transmonlike qubits, see Fig. 6. This architecture is used in "Xmon" qubits [11], for instance. In analogy to the treatment carried out in Sec. II A, we write down the Lagrangian

$$\mathcal{L} = \frac{1}{2}\dot{\mathbf{\Phi}}^T \hat{C}\dot{\mathbf{\Phi}} + E_J \sum_{i=1}^{N} \cos\phi_i, \tag{A1}$$

with capacitance matrix

$$\hat{C} = \begin{pmatrix} C_{\rm sh}+C_c & -C_c & 0 & \cdots \\ -C_c & C_{\rm sh}+2C_c & -C_c & \cdots \\ 0 & -C_c & C_{\rm sh}+2C_c & \cdots \\ \vdots & \vdots & \vdots & \ddots \end{pmatrix}. \tag{A2}$$

Performing a Legendre transformation yields

$$\mathcal{H} = \frac{1}{2}\boldsymbol{q}^T \hat{C}^{-1}\boldsymbol{q} - E_J \sum_{i=1}^{N} \cos\phi_i, \tag{A3}$$

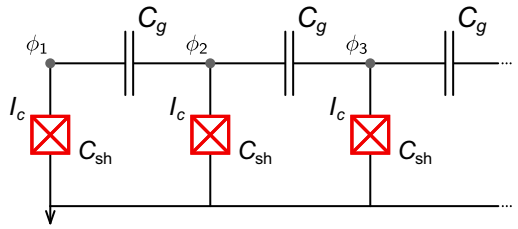

FIG. 6. Schematic circuit diagram for the one-dimensional chain of transmonlike "single-ended" qubits, with one grounded capacitor pad. The qubits are assumed to be identical. Each qubit has one independent circuit node, which has a shunt capacitance $C_{\rm sh}$ to ground and adjacent nodes are coupled with a capacitance C_c.

with the effective capacitance matrix $\hat{C}^g_{\rm eff} \equiv \hat{C}$. The decay of the long-range interactions becomes

$$\frac{J_{i,i+2}}{J_{i,i+1}} = \frac{[\hat{C}_{\rm eff}{}^{-1}]_{i,i+2}}{[\hat{C}_{\rm eff}{}^{-1}]_{i,i+1}} \approx \frac{C_c}{C_{\rm sh}}. \tag{A4}$$

The approximation in Eq. (A4) applies in the realistic regime $C_{\rm sh} \gg C_c$. For typical design parameters of contemporary multiqubit implementations, this ratio is roughly $1/50$.

APPENDIX B: CALCULATION OF COUPLING IN THE STRONG COUPLING REGIME

We analyze here the full solution for the coupling matrix $\mathcal{C}_{\rm eff}{}^{-1}$ for the infinite one-dimensional chain.

The capacitance matrices, defined in Eq. (6) are given by

$$\mathcal{C}^{++}_{ij} = \left[\frac{C_G}{2} + \frac{C_c}{2}\right]\delta_{i,j} - \frac{C_c}{4}\delta_{|i-j|,1}, \tag{B1a}$$

$$\mathcal{C}^{--}_{ij} = \left[C_q + \frac{C_G}{2} + \frac{C_c}{2}\right]\delta_{i,j} + \frac{C_c}{4}\delta_{|i-j|,1}, \tag{B1b}$$

$$\mathcal{C}^{+-}_{ij} = \frac{C_c}{4}(\delta_{i,j+1} - \delta_{j,i+1}), \tag{B1c}$$

where we take $N \to \infty$.

We use the unitary transformation

$$\tilde{\mathcal{C}}^{++}(k,p) = \sum_{i,j} U_i(k)\mathcal{C}^{++}_{ij}U^*_j(p), \quad U_j(p) = e^{-ipj} \tag{B2}$$

to rewrite these in momentum space, finding

$$\tilde{\mathcal{C}}^{++}(k,p) = \delta(k-p)\left(\frac{C_G}{2} + C_c \sin^2\frac{k}{2}\right), \tag{B3a}$$

$$\tilde{\mathcal{C}}^{--}(k,p) = \delta(k-p)\left(C_q + \frac{C_G}{2} + C_c\cos^2\frac{k}{2}\right), \tag{B3b}$$

$$\tilde{\mathcal{C}}^{+-}(k,p) = -i\delta(k-p)\frac{C_c}{2}\sin k. \tag{B3c}$$

As these are diagonal, we can immediately invert them, and we find

$$\mathcal{C}_{\text{eff}}(k,p) = \mathcal{C}^{--} - \mathcal{C}^{-+}(\mathcal{C}^{++})^{-1}\mathcal{C}^{+-} = \delta(k-p)\left[C_q + \frac{\frac{C_G}{2}\left(C_c + \frac{C_G}{2}\right)}{\frac{C_G}{2} + C_c \sin^2\frac{k}{2}}\right], \quad \text{(B4)}$$

$$\mathcal{C}_{\text{eff}}^{-1}(k,p) = \delta(k-p)\frac{1}{C_q} \times \left[1 - \frac{\frac{C_G}{2}\left(C_c + \frac{C_G}{2}\right)}{\frac{C_G}{2}\left(C_q + C_c + \frac{C_G}{2}\right) + C_c C_q \sin^2\frac{k}{2}}\right]. \quad \text{(B5)}$$

We then perform the inverse transformation,

$$\tilde{\mathcal{C}}_{ij}^{++} = \frac{1}{2\pi}\int_{-\pi}^{\pi} dk dp\; U_i^*(k)\mathcal{C}^{++}(k,p)U_j(p), \quad \text{(B6)}$$

to find, in the original lattice basis,

$$(\mathcal{C}_{\text{eff}}^{-1})_{ij} = \frac{1}{C_{q,\text{eff}}}\left[\delta_{i,j}\left(1 + \frac{2\chi}{\xi}\right) - \frac{2\chi}{\xi}\xi^{|i-j|}\right]. \quad \text{(B7)}$$

with

$$C_{q,\text{eff}} = \frac{C_q}{1-\eta_1\eta_2}, \quad \text{(B8a)}$$

$$\xi = \frac{\eta_2 - \eta_1}{\eta_2 + \eta_1}, \quad \text{(B8b)}$$

$$\chi = \frac{\eta_1\eta_2}{2(1-\eta_1\eta_2)}\frac{\eta_2 - \eta_1}{\eta_2 + \eta_1}, \quad \text{(B8c)}$$

where the parameters η_1, η_2 are

$$\eta_1 = \sqrt{\frac{C_G/2}{C_G/2 + C_q}}, \quad \eta_2 = \sqrt{\frac{C_G/2 + C_c}{C_G/2 + C_c + C_q}}. \quad \text{(B9)}$$

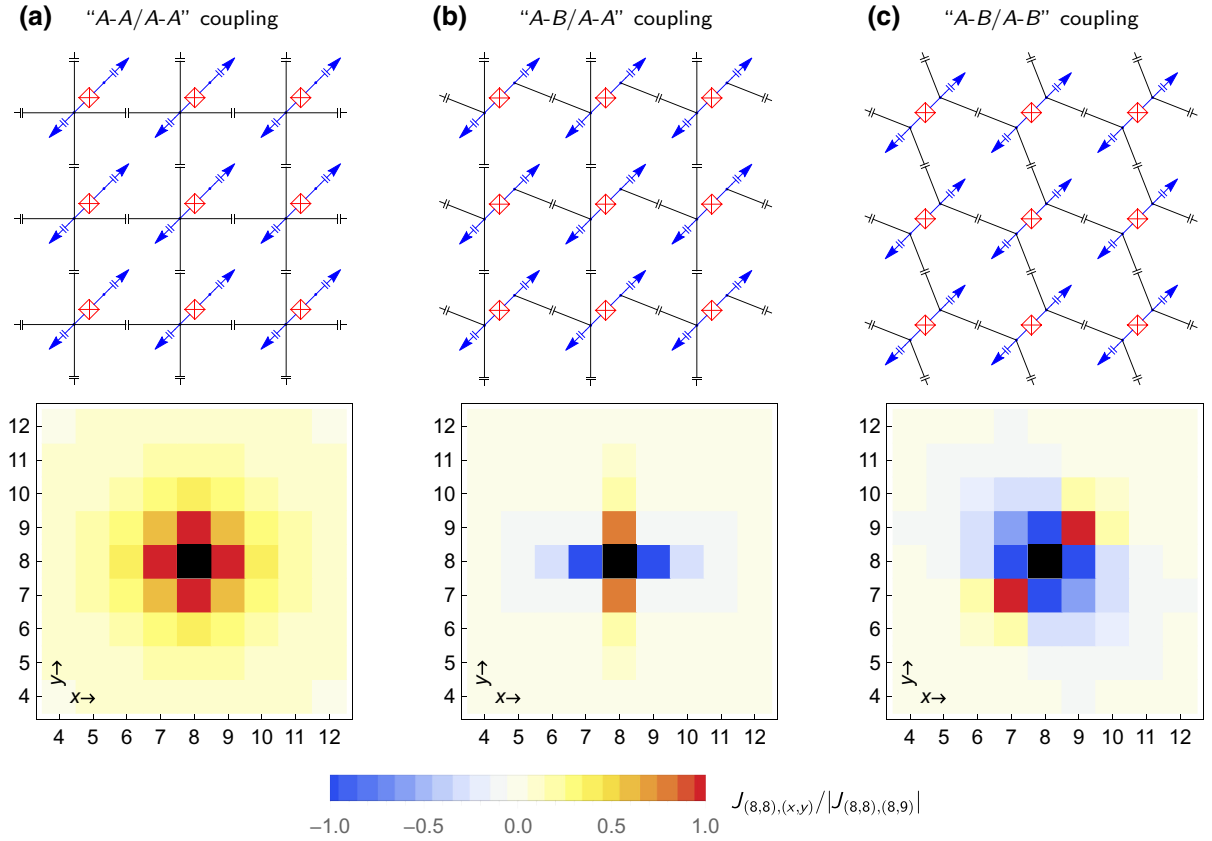

FIG. 7. Nonisotropic couplings in a two-dimensional square lattice. We plot the coupling strength $J_{\mathbf{r}_0,\mathbf{r}}$ between the center qubit $\mathbf{r}_0$ and the rest of the lattice (bottom), normalized to the nearest-neighbor coupling strength, for different coupling typologies (shown at the top). The values are calculated for 15×15 square lattice with $C_c = 0.007C_q, C_G = 0.007C_q$. (a) We observe that the "*A-A*/*A-A*" topology exhibits a simple isotropic form, with $J_{\mathbf{r}_0,\mathbf{r}} \approx \xi^{|\mathbf{r}-\mathbf{r}_0|}$. (b) If the qubits are connected with "*A-B*" form along the one axis and "*A-A*" along the other, we find stronger couplings, with a negative sign, in the "*A-B*" direction, and weaker ones with a positive sign in the "*A-A*" direction. The coupling is suppressed along the diagonals. (c) With "*A-B*" topology in both directions, we find a similar nonisotropic form along the diagonals.

APPENDIX C: CALCULATION OF BOUNDARY EFFECTS ON COUPLING IN A CHAIN

We repeat the calculation in Sec. III, now considering the effects of a final N. The capacitance matrices are now

$$\mathcal{C}_{ij}^{++} = \left[\frac{C_G}{2} + \frac{C_c}{2}(2 - \delta_{i,1} - \delta_{i,N})\right]\delta_{i,j} - \frac{C_c}{4}\delta_{|i-j|,1}, \tag{C1a}$$

$$\mathcal{C}_{ij}^{--} = \left[C_q + \frac{C_G}{2} + \frac{C_c}{4}(2 - \delta_{i,1} - \delta_{i,N})\right]\delta_{i,j} + \frac{C_c}{4}\delta_{|i-j|,1}, \tag{C1b}$$

$$\mathcal{C}_{ij}^{+-} = \frac{C_c}{4}\left[(\delta_{i,N} - \delta_{i,1})\delta_{i,j} + \delta_{i,j+1} - \delta_{j,i+1}\right]. \tag{C1c}$$

To convert into momentum space we use Eq. (20), taking $U_i(k) \to U_{n_k,i}$,

$$U_{nj} = \sqrt{\frac{2 - \delta_{n,0}}{N}}\cos\left[k_n(j - \tfrac{1}{2})\right], \quad k_n = \frac{\pi}{N}n, \tag{C2}$$

for $n = 0, \ldots, N-1$. We find the discrete equivalent of Eq. (21),

$$\mathcal{C}_{nm}^{++} = \delta_{n,m}\left(\frac{C_G}{2} + C_c \sin^2\frac{k_n}{2}\right). \tag{C3}$$

We can immediately invert $\mathcal{C}^{++}$ in momentum space. In the lattice basis, then

$$\begin{aligned}(\mathcal{C}^{++})_{jl}^{-1} &= \sum_{n=0}^{N-1} U_{nj}\frac{1}{\mathcal{C}_{nn}^{++}}U_{nl} \\ &= \frac{1}{2}\sum_n \frac{\cos\left[k_n(j-l)\right] + \cos\left[k_n(j+l-1)\right]}{\frac{C_G}{2} + C_c \sin^2\frac{k_n}{2}}.\end{aligned} \tag{C4}$$

Recalling $k_n = \pi n/N$, for large but finite N we can then approximate this sum as an integral. We must be careful where this approximation breaks down; for $x \sim 2M$, $\cos kx$ varies quickly while $\cos k_n x$ does not. To avoid this, we make use of the equality $\cos\left[k_n x\right] = \cos\left[k_n(2N - x)\right]$ to rewrite the second term in the numerator. We then take $\Delta k_n = \pi/N \to dk$ to find

$$(\mathcal{C}^{++})_{jl}^{-1} \approx \frac{1}{2\pi}\int_{-\pi}^{\pi} dk \frac{e^{ik|j-l|)} + e^{ik(N-|N+1-j-l|)}}{\frac{C_G}{2} + C_c \sin^2\frac{k}{2}}. \tag{C5}$$

Evaluating the integral, we find

$$(\mathcal{C}_{\text{eff}})_{ij} \approx C_q\delta_{i,j} + C_{c,\text{eff}}\left(\xi_C^{|i-j|} - \xi_C^{N-|i+j-N-1|}\right), \tag{C6}$$

with $C_{c,\text{eff}}, \xi_C$ as defined in Eq. (23).

APPENDIX D: 2D LATTICES

While the one-dimensional chain can be described by a simple power-law strength regardless of the circuit form chosen, this is not the case in two dimensions. In Fig. 7 we show how the couplings behave for the different possible circuit topologies of a square lattice.

[1] M. Kjaergaard, M. E. Schwartz, J. Braumüller, P. Krantz, J. I.-J. Wang, S. Gustavsson, and W. D. Oliver, Superconducting qubits: Current state of play, Annu. Rev. Condens. Matter Phys. **11**, 369 (2020).

[2] F. Arute, *et al.*, Quantum supremacy using a programmable superconducting processor, Nature **574**, 505 (2019).

[3] C. K. Andersen, A. Remm, S. Lazar, S. Krinner, N. Lacroix, G. J. Norris, M. Gabureac, C. Eichler, and A. Wallraff, Repeated quantum error detection in a surface code, Nat. Phys. **16**, 875 (2020).

[4] R. Ma, B. Saxberg, C. Owens, N. Leung, Y. Lu, J. Simon, and D. I. Schuster, A dissipatively stabilized Mott insulator of photons, Nature **566**, 51 (2019).

[5] Y. Ye, *et al.*, Propagation and Localization of Collective Excitations on a 24-Qubit Superconducting Processor, Phys. Rev. Lett. **123**, 050502 (2019).

[6] Z. Yan, *et al.*, Strongly correlated quantum walks with a 12-qubit superconducting processor, Science (2019),.

[7] B. Chiaro, *et al.*, Growth and preservation of entanglement in a many-body localized system, (2019), ArXiv:1910.06024.

[8] S. K. Moore, IBM Edges Closer to Quantum Supremacy with 50-Qubit Processor, IEEE Spectrum (2017).

[9] C. T. Rigetti, The Rigetti 128-qubit chip and what it means for quantum (2018).

[10] F. Yan, D. Campbell, P. Krantz, M. Kjaergaard, D. Kim, J. L. Yoder, D. Hover, A. Sears, A. J. Kerman, T. P. Orlando, S. Gustavsson, and W. D. Oliver, Distinguishing Coherent and Thermal Photon Noise in a Circuit Quantum Electrodynamical System, Phys. Rev. Lett. **120**, 260504 (2018).

[11] R. Barends, J. Kelly, A. Megrant, D. Sank, E. Jeffrey, Y. Chen, Y. Yin, B. Chiaro, J. Mutus, C. Neill, P. O'Malley, P. Roushan, J. Wenner, T. White, A. N. Cleland, and J. M. Martinis, Coherent Josephson Qubit Suitable for Scalable Quantum Integrated Circuits, Phys. Rev. Lett. **111**, 080502 (2013).

[12] J. Braumüller, A. H. Karamlou, Y. Yanay, B. Kannan, D. Kim, M. Kjaergaard, A. Melville, B. M. Niedzielski, Y. Sung, A. Vepsäläinen, R. Winik, J. L. Yoder, T. P. Orlando, S. Gustavsson, C. Tahan, and W. D. Oliver, Probing quantum information propagation with out-of-time-ordered correlators, Nat. Phys. **18**, 172 (2021).

[13] M. Dalmonte, M. Di Dio, L. Barbiero, and F. Ortolani, Homogeneous and inhomogeneous magnetic phases of constrained dipolar bosons, Phys. Rev. B **83**, 155110 (2011).

[14] E. Farhi, J. Goldstone, and S. Gutmann, A Quantum Approximate Optimization Algorithm, (2014), ArXiv:1411.4028.

[15] K.-M. Li, H. Dong, C. Song, and H. Wang, Approaching the chaotic regime with a fully connected superconducting quantum processor, Phys. Rev. A **100**, 062302 (2019).
[16] J. Biddle, D. J. Priour, B. Wang, and S. Das Sarma, Localization in one-dimensional lattices with non-nearest-neighbor hopping: Generalized Anderson and Aubry-André models, Phys. Rev. B **83**, 075105 (2011).
[17] D.-L. Deng, S. Ganeshan, X. Li, R. Modak, S. Mukerjee, and J. H. Pixley, Many-body localization in incommensurate models with a mobility edge, Ann. Phys. **529**, 1600399 (2017).
[18] X. Li and S. Das Sarma, Mobility edge and intermediate phase in one-dimensional incommensurate lattice potentials, Phys. Rev. B **101**, 064203 (2020).
[19] S. Xu, Long-range coupling affects entanglement dynamics, Physics **15**, 2 (2022).
[20] H. P. Lüschen, S. Scherg, T. Kohlert, M. Schreiber, P. Bordia, X. Li, S. Das Sarma, and I. Bloch, Single-Particle Mobility Edge in a One-Dimensional Quasiperiodic Optical Lattice, Phys. Rev. Lett. **120**, 160404 (2018).
[21] T. Kohlert, S. Scherg, X. Li, H. P. Lüschen, S. Das Sarma, I. Bloch, and M. Aidelsburger, Observation of Many-Body Localization in a One-Dimensional System with a Single-Particle Mobility Edge, Phys. Rev. Lett. **122**, 170403 (2019).
[22] J. Koch, T. M. Yu, J. Gambetta, A. A. Houck, D. I. Schuster, J. Majer, A. Blais, M. H. Devoret, S. M. Girvin, and R. J. Schoelkopf, Charge-insensitive qubit design derived from the Cooper pair box, Phys. Rev. A **76**, 042319 (2007).
[23] F. Yan, S. Gustavsson, A. Kamal, J. Birenbaum, A. P. Sears, D. Hover, T. J. Gudmundsen, D. Rosenberg, G. Samach, S. Weber, J. L. Yoder, T. P. Orlando, J. Clarke, A. J. Kerman, and W. D. Oliver, The flux qubit revisited to enhance coherence and reproducibility, Nat. Commun. **7**, 12964 (2016).
[24] U. Vool, S. Shankar, S. O. Mundhada, N. Ofek, A. Narla, K. Sliwa, E. Zalys-Geller, Y. Liu, L. Frunzio, R. J. Schoelkopf, S. M. Girvin, and M. H. Devoret, Continuous Quantum Nondemolition Measurement of the Transverse Component of a Qubit, Phys. Rev. Lett. **117**, 133601 (2016).
[25] V. E. Manucharyan, J. Koch, L. I. Glazman, and M. H. Devoret, Fluxonium: Single cooper-pair circuit free of charge offsets, Science **326**, 113 (2009).
[26] P. Brooks, A. Kitaev, and J. Preskill, Protected gates for superconducting qubits, Phys. Rev. A **87**, 052306 (2013).
[27] S. E. Nigg, H. Paik, B. Vlastakis, G. Kirchmair, S. Shankar, L. Frunzio, M. H. Devoret, R. J. Schoelkopf, and S. M. Girvin, Black-Box Superconducting Circuit Quantization, Phys. Rev. Lett. **108**, 240502 (2012).
[28] F. Solgun, D. P. DiVincenzo, and J. M. Gambetta, Simple impedance response formulas for the dispersive interaction rates in the effective hamiltonians of low anharmonicity superconducting qubits, IEEE Trans. Microw. Theory Tech. **67**, 928 (2019).
[29] J. M. Deutsch, Eigenstate thermalization hypothesis, Rep. Prog. Phys. **81**, 082001 (2018).
[30] T. Barthel and U. Schollwöck, Dephasing and the Steady State in Quantum Many-Particle Systems, Phys. Rev. Lett. **100**, 100601 (2008).
[31] F. H. L. Essler and M. Fagotti, Quench dynamics and relaxation in isolated integrable quantum spin chains, J. Stat. Mech. **2016**, 064002 (2016).
[32] T. Kinoshita, T. Wenger, and D. S. Weiss, A quantum Newton's cradle, Nature **440**, 900 (2006).
[33] A. Polkovnikov, K. Sengupta, A. Silva, and M. Vengalattore, Colloquium: Nonequilibrium dynamics of closed interacting quantum systems, Rev. Mod. Phys. **83**, 863 (2011).
[34] J. Eisert, M. Friesdorf, and C. Gogolin, Quantum many-body systems out of equilibrium, Nat. Phys. **11**, 124 (2015).
[35] A. M. Kaufman, M. E. Tai, A. Lukin, M. Rispoli, R. Schittko, P. M. Preiss, and M. Greiner, Quantum thermalization through entanglement in an isolated many-body system, Science **353**, 6301 (2016).
[36] P. Calabrese, F. H. L. Essler, and G. Mussardo, Introduction to 'quantum integrability in out of equilibrium systems', J. Stat. Mech. **2016**, 064001 (2016).
[37] C. E. Porter and R. G. Thomas, Fluctuations of nuclear reaction widths, Phys. Rev. **104**, 483 (1956).
[38] C. Neill, *et al.*, A blueprint for demonstrating quantum supremacy with superconducting qubits, Science **360**, 195 (2018).
[39] D. Yuan, S.-Y. Zhang, Y. Wang, L.-M. Duan, and D.-L. Deng, Quantum Information Scrambling in Quantum Many-body Scarred Systems, (2022), ArXiv:2201.01777.
[40] C. B. Whan, J. White, and T. P. Orlando, Full capacitance matrix of coupled quantum dot arrays: Static and dynamical effects, Appl. Phys. Lett. **68**, 2996 (1996).